

Article

Flexible Helicoids, Atomic Force Microscopy (AFM) Cantilevers in High Mode Vibration, and Concave Notch Hinges in Precision Measurements and Research

Yakov Tseytlin

International Society of Automation (ISA), 20 Randall St., Apt.5G, Providence, Rhode Island 02904, USA; E-Mail: yakovtseyt@aol.com

Received: 27 March 2012; in revised form: 30 April 2012 / Accepted: 11 May 2012 /

Published: 16 May 2012

Abstract: Flexible structures are the main components in many precision measuring and research systems. They provide miniaturization, repeatability, minimal damping, low measuring forces, and very high resolution. This article focuses on the modeling, development, and comparison of three typical flexible micro- nano-structures: flexible helicoids, atomic force microscopy (AFM) cantilevers, and concave notch hinges. Our theory yields results which allow us to increase the accuracy and functionality of these structures in new fields of application such as the modeling of helicoidal DNA molecules' mechanics, the definition of instantaneous center of rotation in concave flexure notch hinges, and the estimation of the increase of spring constants and resolution at higher mode vibration in AFM cantilevers with an additional concentrated and end extended mass. We developed the original kinetostatic, reverse conformal mapping of approximating contours, and non-linear thermomechanical fluctuation methods for calculation, comparison, and research of the micromechanical structures. These methods simplify complicated solutions in micro elasticity but provide them with necessary accuracy. All our calculation results in this article and in all corresponding referenced author's publications are in a good agreement with experimental and finite element modeling data within 10% or less.

Keywords: micro-flexures; helicoids; cantilevers; concave hinges; DNA model; scale factor

1. Introduction

Flexible micro- and nano-helicoids are very sensitive to the stretching force and ambient temperature under which the helicoid proportionally untwists. These structures provide the basis for the design of

extensometers, thermometers, precision measuring heads with visual readout at minimum resolution of order 50 nm, photoelectric automata for dimensional sorting with the measurement rate up to 10 measurement per second, and vibrating string transducers (multivibrators) with minimum resolution of order 5 nm [1]. This structure of twisted strips was first introduced in 1890 by J. Perry who attempted unsuccessfully to develop a theoretical model of the device [2]. A large role in the original mass production of the measurement instruments with pretwisted strips—“mikrokators” in 20 century was played by Swedish company Johansson Gage Co. Photoelectric transducers with pretwisted strips for sorting automata were produced at the Leningrad Instrumental Plant in Russia. Spring measuring heads with pretwisted strips and increased measuring range by the elastic compensator at decreased amplification rate and with multi-revolution pretwisted strip structure at the double end pointer were also developed in that Plant. A large set of the linear and non-linear, quasi-static and dynamic theoretical relations and experimental research of the structure with the pretwisted strips (flexible helicoids) was developed by the author of this paper in the 1960’s and 70’s [1,3]. Despite the decline in production of such systems in recent years due to the development of electronic systems with wide measurement range (inductive, capacitive) and atomic force microscopes (AFM) with micro-nano-cantilevers in quasi-static deformation, natural vibration and vibration at higher modes, flexible helicoidal strips continue to be of interest and use. For example, recently the present author designed a model of DNA molecules using the same helicoidal structure.

We consider in this paper the remaining problems with DNA nano-helicoidal model and vibrating helicoids the largest attainable frequencies, AFM cantilevers at the higher mode of vibration, and concave flexure hinges rotational compliance and instantaneous center of rotation in compliant micro mechanisms and MEMS. A combined presentation of these devices in one article allows us to compare their features in the case of possible application to the measurement and research.

2. Flexure and Stiffness of DNA Nano-Helicoidal Model

In our previous study [4], we built an effective DNA helicoidal model, which reflects many mechanical features of DNA molecules including a possible overwinding and the nonlinear variance of thermomechanical molecular length fluctuations. Nonlinear unwinding and the thermomechanical length L_c fluctuation variance $Var(L_c)$ of DNA molecules were found in the experimental studies at “remeasuring the double helix” [5–7]. Our model (Figure 1(a)) with the hollow pretwisted nanostrip sensor has those features. The length fluctuations correspond to the normal statistical distribution and are in agreement with the equipartition theorem. Hence,

$$Var(L_c) = \Psi k_B T / j_s \tag{1}$$

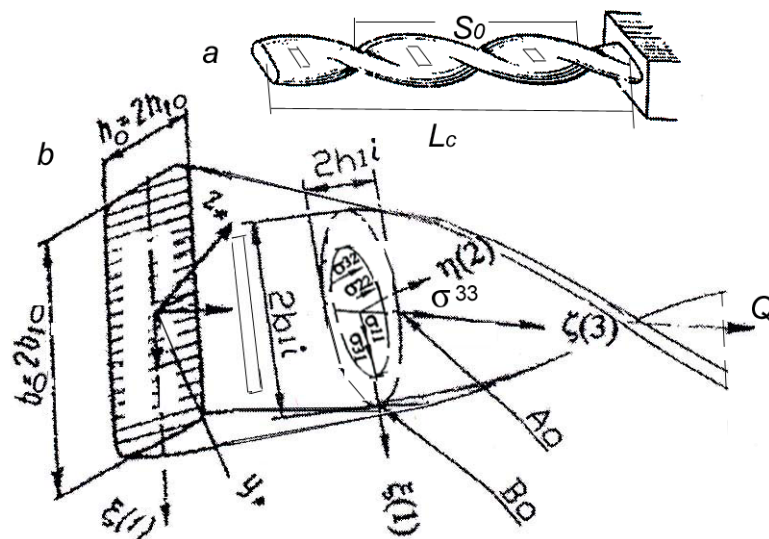
where $\Psi = 170$ is units conversion factor between the left and right sides of the formula in our calculations, k_B is Boltzmann’s constant, T is the absolute temperature in K, and j_s is the object stiffness.

We have previously derived an equation for the pretwisted nanostrip DNA model stretch nonlinear stiffness j_s as the product of the nonlinear average transformation ratio $i_{\theta v}$ and the torsional rigidity j_θ at the pretwisted strip extension. The inverse value of nonlinear stiffness j_s^{-1} therefore [4] is given by:

$$j_s^{-1} = \frac{L_c [1 + \nu_{if} (1 + \nu_H)^2 \chi_{kp} + 3(1 + \nu_H) \nu_H \chi_{kp} / 8]}{E_{e2} [(1 + \nu_H) + \nu_H - 3k_{p0}^2 (1 + \nu_H)^2 \nu_H b_{10}^2] (1 + \nu_{if} \chi_{kp}) A_{cDNA2}} \tag{2}$$

where L_c is the molecular length, $\nu_{jf} = 0.39\text{--}0.41$ is the transformation form coefficient for punched pretwisted nanostrip, $\chi_{kp} = k_{p0}^2(b_o/2)^2\lambda^{-1} = 190.9$ is the dimensionless parameter of the strip's relative pretwist, $\lambda = (h_o/b_o)^2 = 0.0197$ with height $h_o = 0.295$ nm and width $b_o = 2b_{1o} = 2.1$ nm dimensions of the outer rectangular contour (Figure 1(b)), $k_{p0} = 2\pi/S_0 = 1.847$ nm⁻¹ is the initial twist parameter with helical pitch $S_0 = 3.4$ nm, $E_{e2} = 3,470$ pN/nm² is Young's modulus of a DNA molecule in our model, and $A_{cDNA} = 0.317$ nm² is its cross-section area. Note that the product of E_{e2} and A_{cDNA} is equal to 1,100 pN as a so-called stretch modulus. The parameters $\nu_H = -\theta/k_{p0}L_c < 0$ and θ are the stretched strip moving end's rotation relative and absolute angles, respectively. The values of the parameter ν_H are inversely proportional to the molecular length L_c if the angle $\theta = \text{constant}$. Therefore, $\nu_{H1}/\nu_{Hj} = L_{cj}/L_{ci}$.

Figure 1. Pretwisted hollow and punched nanostrip (a), its cross section (b) with helical coordinates $\zeta(1)$, $\eta(2)$, $\zeta(3)$, following coordinates Z^* , Y^* , dimensions $b_o = 2b_{1o} = 2.1$ nm, $b_i = 2b_{1i} = 1.75$ nm are widths, $h_o = 2h_{1o} = 0.295$ nm, $h_i = 2h_{1i} = 0.22$ nm are heights, $S_0 = 3.4$ nm is the helix pitch, L_c is the contour length, σ^{ij} are components of stress tensor for calculation limits of motion and overwinds [4], and A_0 and B_0 are the points of a maximum stress.



3. Scale Parameters of DNA Model Definition

3.1. Stretch Stiffness Relations

The rigidity form coefficient

$$\nu_{jf} = (1/2)[0.1052(1 + \nu_p) + (1 + \nu_p)/8] \tag{3}$$

is given as the average of the corresponding coefficients [1] for rectangular (outer) and elliptical (inner) contours. We recall that Poisson's ratio $|\nu_p|$ for different materials can be in the range 0.0–0.5. The latter value of 0.5 was assumed for our calculations in [4]. However, the real value of ν_{jf} and subsequently Poisson's ratio ν_p can be verified through the experimental measurement of the DNA molecule's stretch stiffness $j_{sp} = dF/ds$, where $F = Q$ (Figure 1(b)) is a stretching force and s is the strip's corresponding stretch. In this case, we can use the simplified linear relations for the transformation ratio i_θ and rotational stiffness $j_{\theta\theta}$ which are equal [1] to:

$$i_{\theta} = -\frac{0.0286 E \kappa_{po}}{4G\lambda(1+v_{if}\chi_{kp})} \tag{4}$$

$$\text{and } j_{\theta} \approx 69.6 G A_{cDNA} \lambda (1 + v_{if}\chi_{kp})/L_c \kappa_{p0} \tag{5}$$

where G is the shear modulus of material.

As a result, the v_{if} value can be deduced (after multiplication and certain cancellations) as follows:

$$v_{if} = \left[\frac{j_{sp}(1+v_{if}\chi_{kp})L_c}{0.498E_{e2}A_{cDNA}} - 1 \right] \chi_{kp}^{-1} \tag{6}$$

Here we assume $v_{if} = 0.41$. If we assume from [8] that for nicked DNA with released torsion in the strand $j_{sp} = 27 \text{ pN/nm} = 65/(0.7 \times 3.4)$ and $L_c = 6.93 \text{ nm}$ as in the first line on the top in Table 1 for the version b^* , then

$$v_{if} = \left[\frac{27(1+0.41 \times 190.9) \times 6.93}{0.498 \times 3470 \times 0.317} - 1 \right] \times 190.9^{-1} = 0.14$$

and from Equation (3) $|v_p| = \frac{2 \times 0.14}{0.2302} - 1 = 0.2$.

Table 1. Thermomechanical variance of DNA molecule’s length L_c at $T = 293 \text{ K}$, $\theta = 1/1.57 = 0.64 \text{ rad}$; $v_{if} = 0.39\text{--}0.41$.

N^o	Calculation (1), (2), (3)						Experiment				$ \delta $ (%)	
	v_H		L_c (Å)		Var (Å ²)		L_c (Å)		Var (Å ²)			
	a	b^*	a	b^*	a	b^*	ae	b^*e	ae	b^*e	a	b^*
1	-0.35	-0.284	56.4	69.3	8.4	16.97	56.4	69.3	8.7	15.8	3.4	7.4
2	-0.228	-0.210	86.1	93.4	22.5	33.2	86.1	93.4	21.2	34.0	6.1	2.3
3	-0.194	-0.206	103.4	95.3	27.9	34.6	103.4	95.3	28.4	34.5	1.8	0.4
4	-0.167	-0.205	121.4	95.8	43.4	35.05	121.4	95.8	42.4	35.0	2.4	0.1
5	-0.15	-0.203	131.1	97.4	51.5	36.0	131.1	97.4	49.4	35.4	4.2	1.7

Version a $v_{if} = 0.18$, experimental ae after [5,6]; version b^* $v_{if} = 0.14$, experimental b^*e after [7].

3.2. Persistence Length Relations

The conditional Poisson’s ratio of DNA may be related to its persistence length A_{bp} as well if we assume (similar to [8,9]) the following expression for the latter:

$$A_{bp} = E_{e2}' J_{\eta} / [n_{bp} (k_B T)] \tag{7}$$

where $E_{e2}' = E_{e2}/(1 - v_p^2)$ is an appropriately modified elastic modulus for the strip bending, $J_{\eta} = \frac{1}{2}(J_{\eta o} - J_{\eta i}) \approx (b_o^3 h_o/24) - (\pi b_i^3 h_i/128) = 0.085 \text{ nm}^4$ is the moment of inertia for the hollow cross section (Figure 1(b)) of the model with pretwisted strip. We also assume that at different conditions (including temperature, type of solution) the value of n_{bp} should be $\sqrt{2}$ or 2 for the helix body with two surfaces: outer (o) and inner (i). This follows from the possible combination of thermomechanical statistical influence on the two surfaces as $\sqrt{(k_B T)^2 + (k_B T)^2} = (k_B T)\sqrt{2}$ or from a necessary thermomechanical energy $2(k_B T)$ at larger material deformation with larger $|v_p|$. Our experience with the published experimental data [5–7] shows that the first value $n_{bp} = \sqrt{2}$ is more

appropriate for a molecule with $\nu_p \leq 0.2$, $\nu_{jf} = 0.14$ and the second value $n_{bp} = 2$ for a molecule with $\nu_p = 0.5$, $\nu_{jf} = 0.18$ in standard solution with 70 mM Tris-HI, pH 8.0 and 10 mM ascorbic acid. Equation (7) yields persistence length values at $T = 293$ K within 49–53 nm for both cases. In any case, the experimental value of j_{sp} and A_{bp} should preferably be measured or evaluated at the corresponding conditions because the persistence length depends on them [7,10] as well as on the molecular length [11]. A mean experimental value of the DNA persistence length in different cases and different solutions is equal to $A_{bp} = (30 + 80)/2 = 55$ nm. The value of ν_{jf} is indeed a scale factor in Equation (2) which can and should be verified on an experimental and theoretical basis for certain representative point of the function in evaluation.

In accordance with Equation (7), the relevant Poisson’s ratio may be found from the following expression:

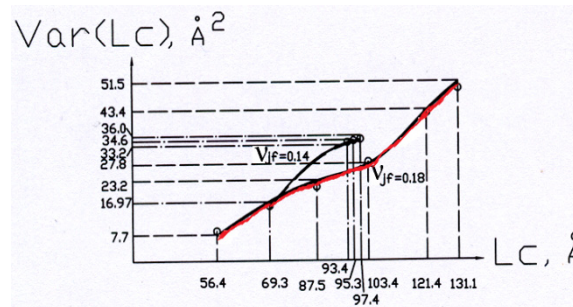
$$\nu_p = \sqrt{1 - \frac{E e^{2J} \eta}{A_{bp} n_{bp} (k_B T)}} \tag{8}$$

4. Calculation Results for DNA Model

Table 1 shows the results of our calculations using Equations (1), (2), and (3) and assuming $\nu_H (L_c = 131.1 \text{ \AA}) = -0.15$, $\nu_{jf}(\nu_p = 0.5) = 0.18$ for version *a*. The difference, $|\delta|$ %, between the calculated and experimental values [5,6] is less than 10%. These data are also represented in Figure 2 where the solid red line ($\nu_{jf} = 0.18$) denotes the calculated results and circles correspond to the experimental values [5,6]. Another set of experimental data [7] in Table 1 for version *b** with $\nu_{jf} = 0.14$ at $\nu_p = 0.2$ also agrees well with the calculation using Equation (1) and is shown in Figure 2. For example, a DNA molecule in the standard buffer solution plus 200 mM NaCl has a persistence length 50 nm [7], while in the standard buffer solution with 0 mM NaCl the persistence length is $A_{bp} = 55.2$ nm. Hence the average $A_{bp} = 52.6$ nm. The experimental variance [7] is $\text{Var}(L_c) = 35.0 \text{ \AA}^2$ at the length $L_c = 95.8 \text{ \AA}$. Calculations with Equation (1) at $L_c = 95.8 \text{ \AA}$, $\nu_H = -0.205$, and $\nu_{jf} = 0.14$ show a variance value of 35.05 \AA^2 which corresponds to the above experimental data with an uncertainty within 0.15%. Calculations with Equation (1) at $L_c = 97.4 \text{ \AA}$, $\nu_H = -0.203$, and $\nu_{jf} = 0.14$ show a variance value of 35.9997 \AA^2 which corresponds to the experimental result [7] of 34.9 \AA^2 with an uncertainty within 3.1% (see the solid line in Figure 2 with $\nu_{jf} = 0.14$). Our calculations with Equation (1) for $L_c = 69.3 \text{ \AA}$ at $\nu_H = -0.2838$ and $\nu_{jf} = 0.14$ show a variance of $\text{Var}(L_c) = 16.97 \text{ \AA}^2$ which corresponds to the experimental data within 7.4%.

Results of this research show that our DNA helicoidal model works well for the evaluation of the nonlinear variance of the molecular length thermomechanical fluctuations in different solutions with an appropriate estimation of a conditional Poisson’s ratio, persistence length, and stretch spring constant of the DNA molecule. Here we have effective relations between the model scale parameters and the functioning conditions of DNA molecules. This research shows the close related features of nano-helicoidal structure in organic and inorganic field.

Figure 2. Thermomechanical variance of the molecular length with solid lines corresponding to our theory for cases with $v_{jf} = 0.14$ and 0.18 (red line), and experimental data denoted by circles.

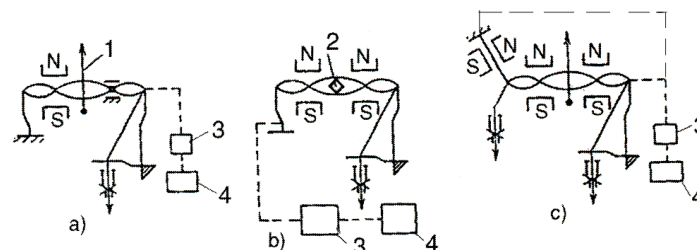


5. Vibrating Transducers

5.1. The Helicoidal Pretwisted String

Helicoidal pretwisted strings have been used by us in so-called helicoidal multivibrators (Figure 3(a–c)). In all cases, the pretwisted bronze strip-string passes through the poles NS of the permanent magnet which generates Lorentz force acting on the string in transverse direction when the electrical pulses from self-oscillator are applied to it. The change of string vibration frequency on the quasi-linear part of the transformation function in this case is proportional to the change of string’s tension. The latter, of course, is proportional to a measurand. The self-oscillators 3 are built as the operational amplifiers with positive feedback to the pretwisted strip and connection to the frequency (oscillation period) meters 4.

Figure 3. Double helicoidal multivibrators with (a) the pointer-arrow 1 on the string; (b) mirror-pointer 2 on the string; (c) differential type of helicoid-cable version [1], self oscillator 3, and frequency meter 4 (reprint from [1], presented with the Springer permission).



The natural frequency of the pointer-arrow rotation on the pretwisted string is nearly 30 Hz, while the small (0.5 mg) mirror–pointer has natural frequency nearly 100 Hz. The working range of a string transducer we built with the pretwisted string is within 2,000–5,000 Hz at the string stretching within 24 μm for the version (Figure 3(b)) and corresponding rotation of the mirror within 90 (angular degree). Large difference in the pointer and the string frequencies guarantees a stable position of the pointer on the dial at the string vibration. As a result, we have a combination of a visual and electrical output on this system which is helpful for measurement purposes and calibration. The minimum spring constant in these structures of zinc bronze ($G = 4.4 \text{ cN/mm}^2$) in accordance with Equation (5) for strings with cross section $0.002 \times 0.06 \text{ mm}^2$, length $L = 20 \text{ mm}$ and pitch $S_0 = 2 \text{ mm}$ is equal to $0.01 \text{ cN}/(\text{angular degree})$.

The pretwisted string has a lower longitudinal rigidity (stiffness) than the flat string with the same dimensions, shape of the cross section, and made of the same material. Therefore, the maximum attainable natural frequencies for the helicoidal strings are lower as well. This is easy to show, for example, on the basis of the helicoidal multivibrator. If the maximum attainable natural frequency for the flat string equals $f_{nmax} = (n_f/2L) \sqrt{\{\sigma_e\}/\rho_\gamma}$, then for the helicoidal multivibrator we have the largest attainable natural frequency, which is equal to:

$$f_{nmax} \approx = (n_f/2L) \sqrt{0.36j_\theta \theta_{lim}/\rho_\gamma A}$$

where n_f is the harmonic number.

Here θ_{lim} is the limit of untwist angle for the pretwisted strip used in the helicoidal multivibrator; j_θ is the pretwisted strip stiffness at the longitudinal extension (in cN per angular degree), and A is the area of the strip's cross section. Substituting the expressions for θ_{lim} and j_θ yields the calculation formula for the attainable largest natural frequency in the helicoidal multivibrator such as

$$f_{nmax} \approx (n_f/2L) \sqrt{A_e/B_e}$$

where $A_e = \{\sigma_e\}25.6(1+\nu_{jf}\chi_{kp})$ and $B_e = \rho_\gamma 8\pi(1+0.38\chi_{kp})$, $\{\sigma_e\}$ is a permissible yield stress for the string's material, ρ_γ is its specific gravity, $\nu_{jf}=(1+\nu_p)/8$ is a coefficient of form rigidity as for an elliptical cross section.

Hence, for the used pretwisted strips in the helicoidal multivibrator [1] with $\chi_{kp} = 8$ and $\nu_{jf} = 0.18$, we have $f_{nmax} \approx 0.78(n_f/2L) \sqrt{\{\sigma_e\}/\rho_\gamma}$ which corresponds to the lowering of the string's upper limit frequency by 22%. In deriving the relationship, we neglected the nonlinearity in the helicoidal multiplier's characteristics and a very small possible change of its density at the initial elastic-plastic twist. But the above shown lowering of the limit for attainable natural frequency in the helicoidal multivibrator is not important because with the increase of its pretension the sensitivity of the frequency transformation for the longitudinal displacement decreases. This shows that using the range of frequencies, which are close to the maximum attainable one for string, is pointless in the case of the helicoidal multivibrator.

5.2. AFM Cantilevers

AFM cantilevers are the main sensitive part of an atomic force microscope which works in a quasi-static mode and in a vibrating mode as well. Cantilevers in this application may have different shapes: rectangular, "dagger" with sharpen end, V-shaped, triangular, tuning fork tines, and special (T-form, doubled, etc.).

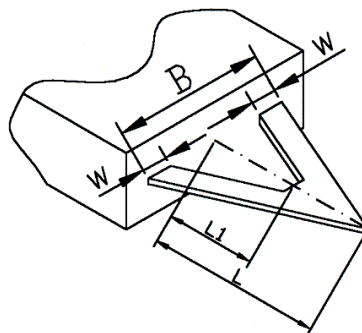
Cantilevers in the vibrating regime are more sensitive to out of plane deformations than in the quasi-static regime, because they have a larger spring constant especially in the higher modes (up to 1,000 times at the fourth mode). This has been found using a kinetostatic method developed by the author [12]. Higher mode oscillations are very sensitive (with resolution of femtogram, attonewton, picometer) to an addition of a small particle close to the end of a cantilever [13] and with atomic resolution in surface parameters measurements. The spring constant of a vibrating cantilever depends on the addition to it of a mass: concentrated, spread, or end expended. The latter is present in a V-shaped cantilever model and causes its specific behavior at vibration in comparison with a rectangular one [14].

The spring constant of AFM cantilevers depends also on the method of their application: permanent contact, non-contact, and tapping mode. Standard micro-cantilevers have small spring constants in a wide range beginning from 0.07 N/m in contact mode that is much lower than for the pretwisted micro-strips. They have larger range of working frequencies up to several megahertz (and nano-cantilevers have frequency up to 1 GHz in vacuum). Therefore AFM cantilevers are more suitable for a surface research with atomic resolution purposes than the pretwisted string transducers. However, we should be careful at the measuring of nano-steps between thin coating and substrate by cantilever at high mode vibration with increased spring constant which can cause increased contact bias [15]. The quasi-unified formula [1] for the fundamental frequency of rectangular, triangular, and V-shaped (Figure 4) cantilever may be presented in simple form as follows:

$$f_0 = \frac{h}{2\pi L^2} \sqrt{\frac{E}{\rho\gamma} \frac{1}{(0.175 + 0.768L_1/L)}} \quad (9)$$

where h is the thickness of a cantilever. One can use this formula for a solid triangular cantilever, if to assume that $L_1 = 0$, and for rectangular cantilever as well if to accept that $L_1 = L$. The calculation results on this basis agree within few percent with the experimental data and more complicated theoretical methods presented in other publications. If these cantilevers are manufactured by lithography from a tape (or sheet) with the constant thickness, we can estimate the block of parameters $h\sqrt{E/\rho\gamma}$ at calibration the frequency f_{c0} of a rectangular cantilever with length L_r and then use the resulting value $h\sqrt{E/\rho\gamma} = 1.942\pi L_r^2 f_{c0}$ for calculation of the fundamental frequency of cantilevers with the other shapes. In this case we don't need to check the real values of thickness, Young's modulus, and specific density of the cantilever separately, especially at a high Q-factor. Equation (9) can be used for cantilevers coated [1] by films of gold, platinum, and even immobilized DNA molecule short ligands as well. Our helicoidal DNA model parameters [4] are especially effective in the latter case.

Figure 4. V-shaped cantilever parameters: L is the length, L_1 is the height of recess, B and w are the width features.



V-shaped cantilevers are widely used in AFM despite the fact that they have more complicated design and some uncertain features of their lateral stability in comparison with rectangular ones, which depends on the geometric parameters and the plane of lateral force application (the height of a tip). V-shaped cantilever can find even more use at higher vibration modes in the atomic force microscopy as a result of improved accuracy in the detection of their deflection by the optical lever because the sign of the slope does not vary along their triangular (trapezoid) part in the incident optical lever area

unlike in rectangular cantilever at higher flexural mode [14], where the nodal points become closer and closer to each other and to the moving end of the rectangular cantilever with the increase of its higher flexural eigenmodes.

AFM cantilevers are very accurate and stable sensors but they require for high resolution much better stability of the environmental conditions (vibration, temperature, humidity, air pressure) than helicoidal micro-sensors.

In both cases, however, the calibration is necessary for the traceability to the primary standards of length and force units as in all precision measurements and research.

6. Concave Flexure Hinges and Their Instantaneous Center of Rotation

Coordinate measuring machines (CMM) and other precision measuring systems with compliant micromechanisms have flexible supports of different kind. Concave notch hinges with cylindrical, elliptic, parabolic, and hyperbolic contours, segmented and V-shaped ones are useful for the purposes of precision measuring and robotic systems miniaturization. Many publications in the scientific and engineering literature have been devoted to the problems of such hinges' accuracy, calibration, and design. However, serious attention to these hinges as a kinematic elements has been developed only recently with the definition of their virtual instantaneous center of rotation (*ICR*) [16]. Let us recall that these elements do not have real guiding surfaces. Therefore, their design and rotational compliance accurate calculation are not effective without the evaluation of the *ICR* position as for rotational joint with the certain stable position of the axis. This evaluation has been found in the author's research on the basis of inverse conformal mapping of approximating contours (Figure 5). An approximating contour in this case is presented by circles R_c shifted l_x from the hinge geometrical center to contiguity with minimum possible deviation from a real concave hinge contour estimated by using Chebyshev's polynomials for uniform or relative approximation. Relative approximation works better for segmented and V-shaped hinges, and their scale factor depends on the ratio between length of straight and curvilinear segments in the contour. The shift l_x was estimated by us in analytical form for cylindrical and elliptic contours and by the three point circle method (circle 3P) in AutoCAD for the hinge contours such as parabolic, hyperbolic, segmented and V-shaped [16,17]. Rotational compliance of these hinges is estimated [1,16] with a following simple unified formula:

$$\alpha_z/M_z = 3(1 - \nu_p)l_x/[4G(\Delta b)^3h_w] \quad (10)$$

where α_z is an angle of rotation at the action of the moment M_z , ν_p is Poisson's ratio, G is a shear modulus of the hinge material, $t = 2\Delta b$ is the thickness, and h_w is the depth of the hinge body. Experimental verification and finite element modeling (FEM) prove the validity of these assumptions with uncertainty within less than 10%.

In general, the position of the *ICR* has some deviation d_{ea} from the geometric center O of a symmetrical notch hinge (Figure 6) that was not considered by many other researchers who supposed that these points always coincide. Our mathematical model for concave notch hinges allows us correct this problem. We showed that $d_{ea} = l_x/2\pi$ for the thin notch hinges with $\Delta b/R \leq 0.035$, $d_{ea} = l_x/3$ for the thick notch hinges with $0.1 < \Delta b/R \leq 0.5$, and $d_{ea} = l_x/5.1$ for the intermediate hinges with $0.035 < \Delta b/R \leq 0.1$. Corresponding adjustment of a clamped to hinge 1 part 2 allows us to find the position of a virtual axis

with *ICR* of the hinge rotation at minimum instability of the cylindrical part O_c axis position during part 2 on the hinge rotation. Eccentric shift D_a in the axis of rotation position in part 2 can cause the change in the effective angle of rotation as $\alpha_{z1} = \alpha_z (1 \pm D_a/\rho)$ and the rotational compliance α_{z1}/M_z estimation. The influence of different heuristic approaches to the problem of *ICR* position on the shift of the rotational axis in the flexure notch hinges is discussed in [18].

Figure 5. Concave contour R with center point O and center line CL approximation by circles R_c with contiguity in point O_1 at shift l_x and applied bending moment $M_b = M_z$ (reprint from [1], presented with the Springer permission).

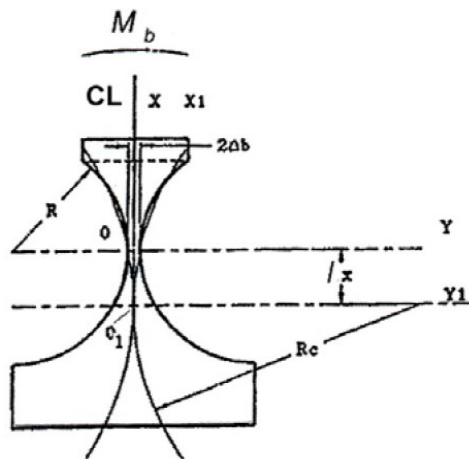
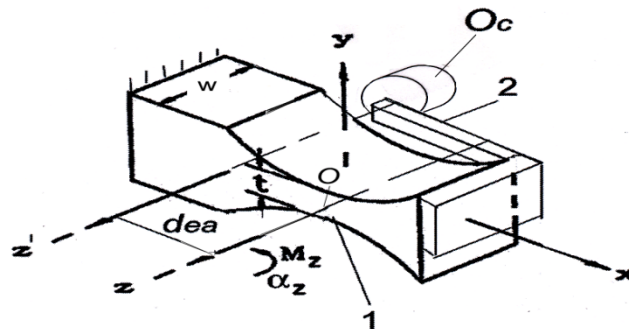


Figure 6. *ICR* of notch hinge1 position on the virtual axis z' rotation in part 2 with cylindrical surface O_c of radius ρ (reprint from [17] with the AIP permission).



Let us recall that the small shift of *ICR* at a finite angle of rotation corresponds to cycloid which is close to semi-cubic parabola. At a finite angle of rotation within $\alpha_z = 0.1$ rad (5.7°), we have a small $X_{ICR} = \alpha_z^3 d_{ea}/6 = 0.00017 d_{ea}$ and $Y_{ICR} = \alpha_z^2 d_{ea}/2 = 0.005 d_{ea}$ shift of *ICR* coordinates from their initial $(-d_{ea}, 0)$ position, which corresponds to the roll without sliding for circle of rolling on the pole tangent [1]. This may be considered in many cases as a practically negligible shift.

7. Conclusions

Flexible pretwisted helicoids, AFM cantilevers, and concave flex notch hinges are the important components of many precision measuring and research systems. Their effective applications have been known for a long time. However, research on their properties and development of their

applications continues to this day. This article presents the author's research results in this field of precision micro elasticity.

Pretwisted helicoids with micro-strings in vibrating mode (helicoidal multivibrators) can be used in the automatic measuring systems with resolution of order 5 nm. Pretwisted nano-strips version is good for the modeling of DNA helicoidal structure with rigidity scale factor and conditional Poisson's ratio estimation on the basis of the molecule stretch stiffness and its persistence length in the corresponding conditions.

AFM cantilevers are very effective in higher vibrating mode with resolution on the order of femtograms, attonewtons, and picometers. Our kinetostatic method allows the evaluation of a cantilever's spring constants increased ratio in the higher vibrating modes with dependence on the connected concentrated and end expanded mass. The latter is especially important for modeling of V-shaped cantilevers by kinetostatic method.

The inverse conformal method of approximating contours is very effective for modeling the rotational compliance of concave flex notch hinges with different contours and the evaluation of the position of their instantaneous center of rotation (*ICR*). The latter was introduced for the first time in mathematical model by the author. It is clear that an accurate calculation of rotational compliance for a concave notch hinge is not effective without a proper its *ICR* definition. The results of all our calculations in this article and referenced publications agree to within less than 10% with experimental data and finite element method (FEM) estimations.

Acknowledgements

The author wishes to acknowledge the helpful editorial assistance of R. Pelcovits.

Reference

1. Tseytlin, Y.M. *Structural Synthesis in Precision Elasticity*; Springer: New York, NY, USA, 2006; p. 397.
2. Perry, J. Twisted strips. *Proc. Phys. Soc. Lond.* **1890**, *XLIV*, 343–349.
3. Tseytlin, Y.M. Computation of spring-loaded instrument mechanism. *Meas. Techniq.* **1965**, *8*, 223–226.
4. Tseytlin, Y.M. An effective model of DNA like helicoid structure: With length fluctuation nonlinearity. *AIP Adv.* **2011**, *1*, 012116:1–012116:6.
5. Mathew-Fenn, R.S.; Das, R.; Harbury, P.A.B. Remeasuring the double helix. *Science* **2008**, *322*, 446–449.
6. Mathew-Fenn, R.S.; Das, R.; Silverman, J.A.; Walker, P.A.; Harbury, P.A.B. A molecular ruler for measuring quantitative distance distribution. *PLoS One* **2008**, *3*, e3229.
7. Mathew-Fenn, R.S.; Das, R.; Fenn, T.D.; Schneiders, M.; Harbury, P.A.B. Response to comment on “Remeasuring the double helix”. *Science* **2009**, doi: 10.1126/science.1168876.
8. Bustamante, C.; Bryant, Z.; Smith, S.B. Ten years of tension: Single-molecule DNA mechanics. *Nature* **2003**, *421*, 423–427.
9. Bodal, D. *Mechanics of the Cell*; Cambridge University Press: London, UK, 2002; p. 406.

10. Dobrynin, A.V. Effect of counterion condensation on rigidity of semiflexible polyelectrolytes. *Macromolecules* **2006**, *39*, 9519–9527.
11. Eslami-Mossallam, B.; Ejtehadi, M.R. Contribution of nonlocal interactions to DNA elasticity. *J. Chem. Phys.* **2011**, *134*, 125106:1–125106:9.
12. Tseytlin, Y.M. Atomic force microscope cantilever spring constant evaluation for higher mode oscillations: A kinetostatic method. *Rev. Sci. Instrum.* **2008**, *79*, 025102:1–025102:7.
13. Tseytlin, Y.M. High resonant mass sensor evaluation: An effective method. *Rev. Sci. Instrum.* **2005**, *76*, 115101:1–115101:6.
14. Tseytlin, Y.M. Kinetostatic model of spring constant ratios for an AFM cantilever with end extended mass. *Ultramicroscopy* **2010**, *110*, 126–129.
15. Tseytlin, Y.M. Nanostep and film-coating thickness traceability. In *Proceedings of the 53 IIS*, Tulsa, OK, USA, 30 April–3 May 2007; Volume 470, Papertp007iis006:1– Papertp007iis006:6.
16. Tseytlin, Y.M. Tractable model for concave flexure hinges. *Rev. Sci. Instrum.* **2011**, *82*, 015106:1–015106:4.
17. Tseytlin, Y. Note: Rotational compliance and instantaneous center of rotation in segmented and V-shaped notch hinges. *Rev. Sci. Instrum.* **2012**, *83*, 026102:1–026102:3.
18. Linß, S.; Erbe, T.; Theska, R.; Zentner, L. The influence of asymmetric flexure hinges on the axis of rotation. In *Proceedings of the 56th International Scientific Colloquium*, Ilmenau University of Technology, Ilmenau, Germany, 12–16 September 2011; p. 10.

© 2012 by the authors; licensee MDPI, Basel, Switzerland. This article is an open access article distributed under the terms and conditions of the Creative Commons Attribution license (<http://creativecommons.org/licenses/by/3.0/>).